Ocean forced variability of Totten Glacier mass loss

JASON ROBERTS[1,2]*, BENJAMIN K. GALTON-FENZI[1,2], FERNANDO S. PAOLO[3], CLAIRE DONNELLY[4], DAVID E. GWYTHER[2,5], LAURIE PADMAN[6], DUNCAN YOUNG[7], ROLAND WARNER[2], JAMIN GREENBAUM[7], HELEN A. FRICKER[3], ANTONY J. PAYNE[4], STEPHEN CORNFORD[4], ANNE LE BROCQ[8], TAS VAN OMMEN[1,2], DON BLANKENSHIP[7] & MARTIN J. SIEGERT[9]

[1]*Australian Antarctic Division, Hobart, Tasmania, Australia*

[2]*Antarctic Climate & Ecosystems Cooperative Research Centre, University of Tasmania, Hobart, Tasmania, Australia*

[3]*Scripps Institution of Oceanography, University of California San Diego, La Jolla, California, USA*

[4]*School of Geographical Sciences, University of Bristol, Bristol, UK*

[5]*Institute for Marine and Antarctic Studies, University of Tasmania, Hobart, Tasmania, Australia*

[6]*Earth & Space Research, Corvallis, Oregon, USA*

[7]*Jackson School of Geosciences, University of Texas at Austin, Austin, Texas, USA*

[8]*School of Geography, University of Exeter, Exeter, Devon, UK*

[9]*Grantham Institute and Department of Earth Science and Engineering, Imperial College London, South Kensington, London, UK*

**Correspondence: Jason.Roberts@aad.gov.au*

Abstract: A large volume of the East Antarctic Ice Sheet drains through the Totten Glacier (TG) and is thought to be a potential source of substantial global sea-level rise over the coming centuries. We show that the surface velocity and height of the floating part of the TG, which buttresses the grounded component, have varied substantially over two decades (1989–2011), with variations in surface height strongly anti-correlated with simulated basal melt rates ($r = 0.70$, $p < 0.05$). Coupled glacier–ice shelf simulations confirm that ice flow and thickness respond to both basal melting of the ice shelf and grounding on bed obstacles. We conclude the observed variability of the TG is primarily ocean-driven. Ocean warming in this region will lead to enhanced ice-sheet dynamism and loss of upstream grounded ice.

The East Antarctic Ice Sheet (EAIS) is the world's largest potential source of sea-level rise (53.3 m; an order of magnitude greater than either West Antarctica or Greenland), with the marine-based component (i.e. where the ice sheet is grounded below sea level) containing enough ice to raise sea levels by 19.2 m (Fretwell *et al.* 2013). The Totten Glacier (TG: see Fig. 1c for the location) has the largest outflow (70 ± 4 km^3 a^{-1}) of any glacier in East Antarctica, and has the third highest ice flux of all Antarctic glaciers, behind only the Pine Island and Thwaites glaciers (Rignot & Thomas 2002), both in the Amundsen Sea (AS) region of West Antarctica. The Aurora Subglacial Basin is an extensive region of grounded ice that drains primarily through the main trunk of the TG (Roberts *et al.* 2011; Young *et al.* 2011; Wright *et al.* 2012) and contains enough marine-based ice to raise the global sea level by 3.5 m (Greenbaum *et al.* 2015). The TG has an extensive embayed floating ice shelf adjoining a weakly grounded 'ice plain' containing topographical features (Li *et al.* 2015) that have previously been interpreted as 'ice rumples', with the ice surface slightly above the flotation limit (Greenbaum *et al.* 2015). It is thought that, by analogy with observed changes in the AS region of West Antarctica (Shepherd & Wingham 2007; Pritchard *et al.* 2009, 2012), these features make the TG susceptible to rapid

From: Siegert, M. J., Jamieson, S. S. R. & White, D. A. (eds) 2018. *Exploration of Subsurface Antarctica: Uncovering Past Changes and Modern Processes*. Geological Society, London, Special Publications, **461**, 175–186.
First published online August 23, 2017, https://doi.org/10.1144/SP461.6

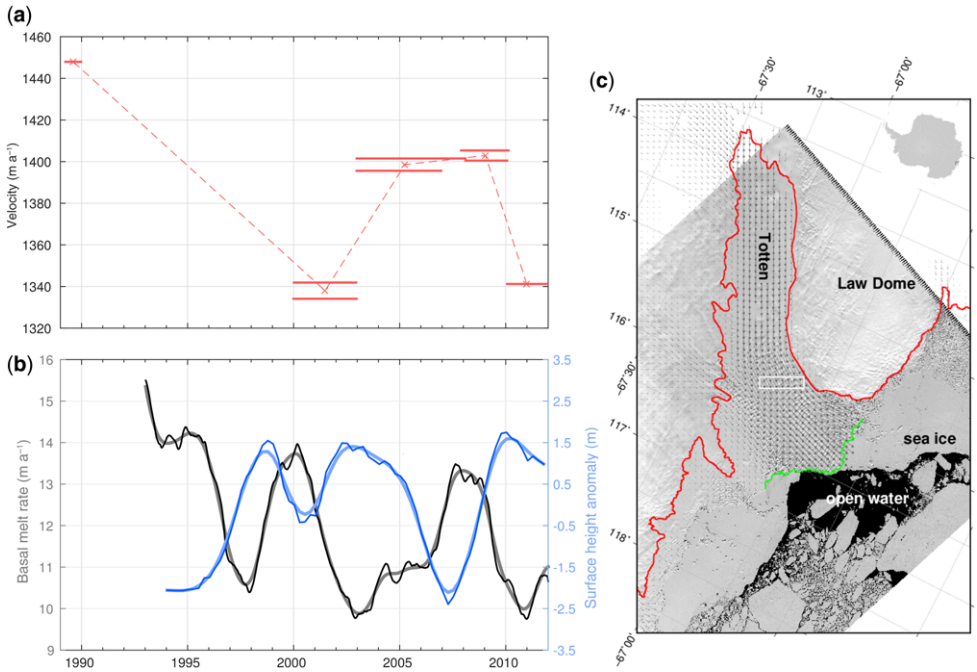

Fig. 1. (**a**) Surface ice velocity from Landsat4 and Landsat7 image pairs, averaged over the region shown in (c) (white box). (**b**) Relative changes in surface height from ERS altimetry data (Paolo *et al.* 2016) (blue) are anti-correlated with computer simulations of melt rate ($r^2 = 0.70$), area-averaged over the TIS. (**c**) Location of the TG, also showing the MEaSUREs velocity field (Rignot *et al.* 2011) (vectors), ASAID ice-sheet grounding line (Bindschadler *et al.* 2011*a*) (red) and the seawards extent of the TG (green). The white box denotes the area for velocity averages shown in (a).

grounding zone retreat via the marine ice-sheet instability mechanism (Schoof 2007) and potentially sensitive to changing ocean conditions (Li *et al.* 2016). Indeed, evidence of past large-scale retreat cycles has been inferred from erosion patterns beneath the ice sheet (Aitken *et al.* 2016), potentially driven by changing ocean conditions.

Analysis of satellite laser-altimeter measurements (ICESat), of relatively short-duration (2003–08), showed a mass-loss trend for the TG, with surface lowering in some regions in excess of 1.9 m a^{-1} (Pritchard *et al.* 2009). Mass balance estimates from accumulation over the catchment basin, and velocities at the grounding line, show the TG catchment was losing ice at a rate of approximately 8 Gt a^{-1} over the period 1992–2006 (Rignot & Thomas 2002; Rignot *et al.* 2008), despite a period of anomalously high regional snowfall (van Ommen & Morgan 2010). Furthermore, analysis of satellite gravity data from the GRACE mission indicated accelerated mass loss of the grounded region from slightly over 2 Gt a^{-1} in mid-2002 to nearly 18 Gt a^{-1} in 2009 (Chen *et al.* 2009). Recent analysis of a longer time series (1994–2012) of surface-height data for the ice shelf revealed large interannual variability in elevation over the floating portion of the TG (Totten Ice Shelf; TIS), with an overall slight negative trend over the full time interval that becomes more pronounced during the ICESat period (Paolo *et al.* 2015).

Here we present further evidence showing that the variability of the TG is apparent in observations of both surface ice velocities and surface height. Numerical ocean modelling indicates that interannual differences in water mass properties in the region can lead to large variations in basal melting of the TIS (Khazendar *et al.* 2013; Gwyther *et al.* 2014), suggesting that both TIS elevations and ice dynamics may be modulated by variability in ocean forcing (Li *et al.* 2016). Thus, the aim of this paper is to provide a mechanism which explains that the variability of the TIS is in response to changes in ocean forcing. This aim will be addressed using both satellite observations and modelling.

Methods

Surface ice velocities

We calculated surface velocities using visible feature tracking techniques for the periods 1989, 1999–2002,

Table 1. *Details of Landsat image pairs used to calculate velocity changes*

Satellite	Path	Row	Date of initial image	Date of final image
Landsat4	102	107	28 March 1989	25 December 1989
Landsat7	101	107	30 December 1999	22 December 2002
Landsat7	101	107	22 December 2002	6 February 2008
Landsat7	101	107	22 December 2002	17 December 2006
Landsat7	102	107	6 January 2000	27 November 2002
Landsat7	102	107	25 November 2007	18 February 2010
Landsat7	102	107	6 January 2000	13 December 2002
Landsat7	101	107	6 February 2008	26 January 2010
Landsat7	101	107	7 May 2010	30 November 2011

2002–08 and 2008–10 from a combination of Landsat4 (1989) and Landsat7 (1999 onwards) image pairs (see Table 1 for details).

Velocities were obtained from fast Fourier transform (FFT)-based correlations derived from surface feature displacements from Landsat4 or Landsat7 image pairs. The images are 'Systematic Terrain Correction' (Level 1GT) products in standard polar stereographic projection (reference latitude 71°S). Level 1GT images are corrected for terrain distortions using the Radarsat Antarctic Mapping Project (RAMP) digital elevation model (DEM), which may introduce potentially large errors. However, as our area of interest is an ice shelf of relatively uniform surface height, we expect any such effects to be small. To further minimize these effects, co-registration of the image pairs was based on persistent features near the edge of the ice sheet, where the ice is thin and surface features are a reflection of the underlying bedrock features. These regions tend to be at broadly similar elevations to the ice shelf.

To account for Scan Line Correction off (SLC-off) problems in 2003–present images, the feature tracking software (Scambos *et al.* 1992) was modified to fill these gaps with random data selected from the intensity histogram for the valid region of the image (Warner & Roberts 2013). To reduce variability, displacements were calculated for 1920 × 1920 m reference 'chips' on a 300 m grid and then binned onto a 1 × 1 km grid based on a least trimmed squares (Rousseeuw & Hubert 1997), requiring at least three data points per bin. To further reduce noise, we only retained data where at least four of the nine neighbouring points had both displacement components within 150 m of each other.

Surface heights

We constructed an 18 year record of ice-shelf height using data from three European Space Agency (ESA) satellite radar altimeter (RA) missions: the European Remote Sensing Satellite-1 and Satellite-2 (ERS-1, 1991–96; and ERS-2, 1995–2011), and the Environmental Satellite (Envisat, 2002–12). We obtained Level-2 RA data as Version 5 Ice Data Records (IDRs) for each mission from the NASA/GSFC (Goddard Space Flight Center) Ice Altimetry Group (http://icesat4.gsfc.nasa.gov/). At GSFC, the RA waveforms were retracked using a range-retracking algorithm that fits a multi-parameter function to each one (the β-retracker) (Zwally & Brenner 2001); one of these parameters is the retracking point, which is the mid-point on the waveform leading edge. The following corrections were applied by GSFC: atmospheric range corrections; instrument corrections; slope corrections; ocean and solid Earth tides (Brenner *et al.* 1983; Zwally & Brenner 2001; Zwally *et al.* 2005); (for ERS) removal of a 0.41 m bias from ERS-1 heights to account for a change in instrument parameter used for ERS-2 (Femenias 1996); corrections for drifts in the ultra-stable oscillator and bias changes in the scanning point target response that are obtained from ESA; and upgraded orbits (DGM-E04 orbits for ERS), which have a radial orbit precision of 0.05–0.06 m (Scharroo & Visser 1998).

Our determination of height changes over the ice shelves from multi-mission satellite RA data is based on 'crossover analysis' (Zwally *et al.* 1989, 2005; Davis & Ferguson 2004; Wingham *et al.* 2009), which estimates change in surface height at intersections between time-separated ascending and descending satellite tracks. The following processing steps were undertaken (Paolo *et al.* 2016): subsetting data over floating ice; data editing and additional corrections required for floating ice and for radar signal interactions with the surface layer on the ice shelves; crossover analysis; methods for merging data records from the different missions; and the averaging scheme required to achieve satisfactory data coverage and accuracy. The output is 18 year-long records of ice-shelf surface height, which we then analysed using statistical techniques to derive long-term trends, acceleration and uncertainties.

Ice sheet/shelf modelling

Ice sheet and shelf modelling was undertaken (Donnelly 2014) with a drainage basin regional model using the BISICLES model (Cornford *et al.* 2013, 2015). The 'full Stokes' equations describing ice dynamics are approximated with a so-called higher-order approximation, with vertically integrated treatment of momentum for computational efficiency. Horizontal grid resolution varies (1–16 km) throughout the computational domain as a function of the ice speed and proximity to the grounding line. The geometry is based on the BEDMAP2 (Fretwell *et al.* 2013) compilation, and an initial thermal state is specified (Pattyn 2010). The applied pattern of ocean-driven melt at the base of the ice shelf is diagnosed from observed ice-flux divergence, with the temporal modulation of melt specified as sinusoidal with a period of 10 years and an amplitude of 0.5 of the temporal average (Donnelly 2014).

Ocean modelling and basal melt

We simulated the ice shelf–ocean interaction with the Regional Ocean Modeling System (ROMS) (Shchpetkin & McWilliams 2005), a finite-difference method ocean model. The primitive equations of fluid flow are discretized on a terrain-following vertical coordinate, allowing for increased resolution near bathymetry/ice-shelf surface and boundary layers. Modifications are included to simulate tides, ice shelves and for ice–ocean thermodynamics (Galton-Fenzi *et al.* 2012). Continental shelf and deep-ocean bathymetry is based on RTOPO (Timmermann *et al.* 2010), while the bathymetry within the TIS cavity is added as a constant offset below the ice draft (inverted from the ice elevation (ICESAT) assuming a representative density of ice and seawater). The model domain (104.5°E–130°E, 68°S–60°S) is forced by relaxation at the lateral (east, north and west) and surface boundaries. See Gwyther *et al.* (2014) for a further description of the model, including set-up, and the forcing and boundary conditions used here.

Two different models using different atmospheric forcing were used. One ocean model simulated 1992–2007 with interannual forcing derived from reanalysis products for the lateral boundaries (ECCO2: Menemenlis *et al.* 2008) and surface (CORE: Large & Yeager 2009) augmented with special sensor microwave/imager algorithms for sea-ice production (Tamura *et al.* 2008), which is described fully in Gwyther *et al.* (2014). This model is spun-up by 16 years of repeated 1992 forcing, at which point the ocean heat content has approximately plateaued. The other model run simulated 1992–2012 conditions with the same finite-difference code, but employed a more modern ECCO2 version, the reanalysis product ERA-Interim (Dee *et al.* 2011), for surface forcing and

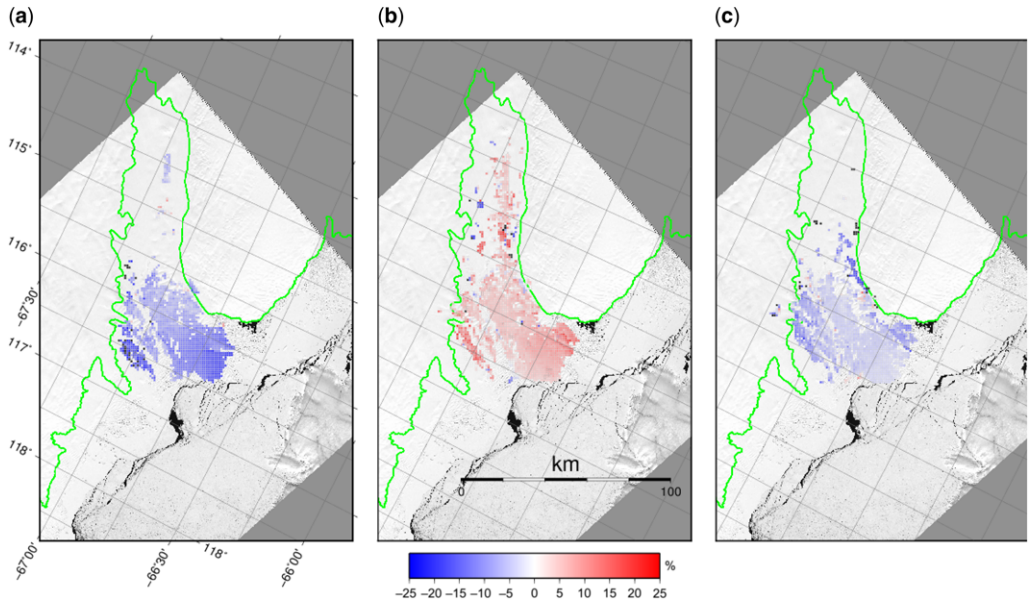

Fig. 2. Change in speed of the TG ice shelf. Difference in speed between image pairs: (**a**) (28 March 1989, 25 December 1989) and (1999, 2002); (**b**) (1999, 2002) and (2008, 2010); and (**c**) (2008, 2010) and (2010, 2011). Also shown is the ASAID grounding line (Bindschadler *et al.* 2011*a*).

updated surface sea-ice production rates. This model was run with two periods of 1992–2012 forcing (42 years in total), with the first period spinning the model up and the second period being used for analysis.

For comparison with the ocean-model solution, basal melt for the TIS was also calculated from ice-penetrating radar thickness profiles (Young *et al.* 2011) and surface ice velocities (Rignot *et al.* 2011). Both datasets were averaged onto the same 1 × 1 km polar stereographic grid. Local mass flux estimates from coincident thickness and velocity data points were advected downstream until reaching the next local mass flux point using a modified version of a the Lagrangian streamline code (Roberts *et al.* 2011), accounting for across-stream convergence/divergence. The mass flux difference between these points was assigned uniformly along the streamline as the average change in mass flux along the streamline. All such estimates for each grid cell where averaged and a 15 km Gaussian filter applied. This represents an estimate of the local basal melt rate, in general an underestimate as surface snowfall will have contributed to the along-streamline mass flux changes.

Results

We analysed a sequence of ice-surface velocity measurements from automated correlation between pairs of co-registered visible-band light satellite images (Scambos *et al.* 1992; Warner & Roberts 2013) over the period 1989–2012. The results show temporal variability in the flow of the TIS during these 24 years, in agreement with mass-budget estimates (Li *et al.* 2016). Between 1989 and 2001, the TIS slowed by over 7%, followed by a 4% speed-up between 2002 and 2009 and another, more tightly constrained, slowdown during 2010–11 of similar magnitude (Fig. 1a). While the lack of suitable satellite imagery leads to sparse temporal coverage, our velocity measurements are of sufficient quality to capture interannual variability (Fig. 2), as it is significantly larger than the uncertainty in each velocity measurement. Ice-shelf speeds in the vicinity of the rumple near the grounding line are in the range of 900–1000 m a^{-1} (Rignot *et al.* 2011). The observed variability of velocity appears linked with an 18 year (1994–2011) record of surface-height change, averaged over the central TIS area (Paolo *et al.* 2015), with an overall trend not significantly different

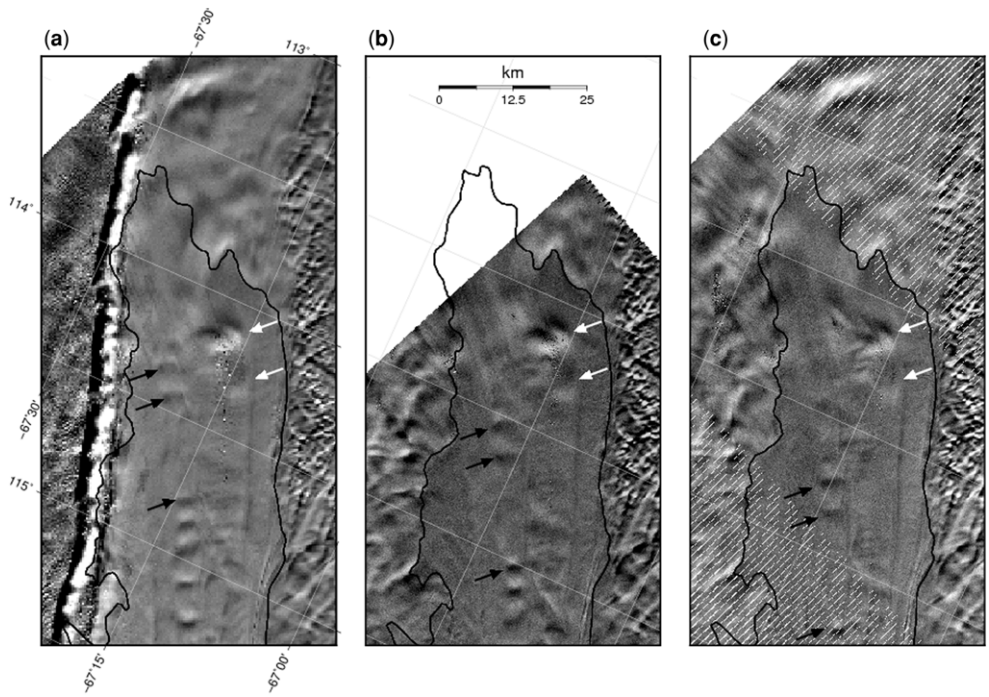

Fig. 3. The TG ice-shelf rumple. Landsat4 and Landsat7 images of the TG ice shelf, also showing the ASAID grounding line (Bindschadler *et al.* 2011*a*) (black line), ice rumples (white arrows) and surface undulations (black arrows): (**a**) 28 March 1989; (**b**) 30 December 1999; and (**c**) 18 February 2010. Data gaps associated with Scan Line Correction Off (SLC-off) problems from 2003 and onwards images are evident.

from zero (Fig. 1b). An approximately 6 year period (2004–09) is characterized by a relatively lower elevation corresponding to the period of faster surface velocities.

Hindcast area-averaged TIS basal melt rates from an ocean model (Gwyther *et al.* 2014), which shows high variability over a 20 year period (1992–2012), are anti-correlated with surface-height variations ($r = 0.70$ with a 95% confidence interval of 0.69–0.71, calculated using a bootstrap method taking into account signal auto-correlation: Ólafsdóttir & Mudelsee 2014). Increased melting leads to a lowering of surface height and vice versa (Fig. 1b), driven primarily by changes in ocean temperature. This result was supported by a second ocean-model simulation, although of a shorter 16 year period, using a different source of hindcast forcing (not shown). The average melt rates for the TIS are 9.1 ± 2.7 m a^{-1} for the 16 year run and 12.1 ± 3.0 m a^{-1} for the 20 year run, in agreement with steady-state mass-budget estimates of 9.2 ± 0.7 m a^{-1} (Rignot *et al.* 2013).

A sequence of three Landsat visible light images separated by approximately a decade and spanning the epoch 1989–2010 (Fig. 3) shows two stationary features (white arrows) downstream of the grounding line at around 67°15′S, which we interpret to be ice rumples (Matsuoka *et al.* 2015), areas where the underlying bedrock shoals, re-grounds the ice shelf and forces the ice to locally rise above hydrostatic equilibrium (but, as distinct from an ice rise, does not result in significant changes in the local flow direction, only its magnitude). This is confirmed by the along-flow strain rate (Fig. 4) calculated by differentiation of surface velocity data (Rignot *et al.* 2011). This shows a region of flow retardation upstream of the rumples, associated with the basal drag there. Furthermore, time-varying basal melt will produce waves of thickness variations (undulations shown by black arrows in Fig. 3) that propagate at the ice-shelf velocity, which is equal to the product of the wavelength of the thickness undulations and their frequency of generation (Fig. 5) (Donnelly 2014). The calculated period of the thickness variation is 6–7 years (Donnelly 2014), based on an estimate of the wavelength from Landsat7 imagery, which will also correspond to the period of variation in the basal melt rate. High melt regions are near the deep grounding line and around the two rumples (Fig. 6a). For comparison, the spatial distribution of average basal melt rate from the 1992–2012 ocean-model simulation is shown in Figure 6b, showing that the regions of highest melt correspond with the deepest ice near the southern grounding zone.

The observed significant anti-correlation between variations in elevation and modelled basal melt rates (Fig. 1b) supports the realism of the timing of the basal melt rates as driven by the time series of forcing fields representing the surrounding atmosphere and ocean. Furthermore, comparing the relative magnitudes of the variations indicates that the melt rates are quite sensitive to the range of natural variability described by the forcing. This basal melt rate variability also influences the ice flow of the TIS.

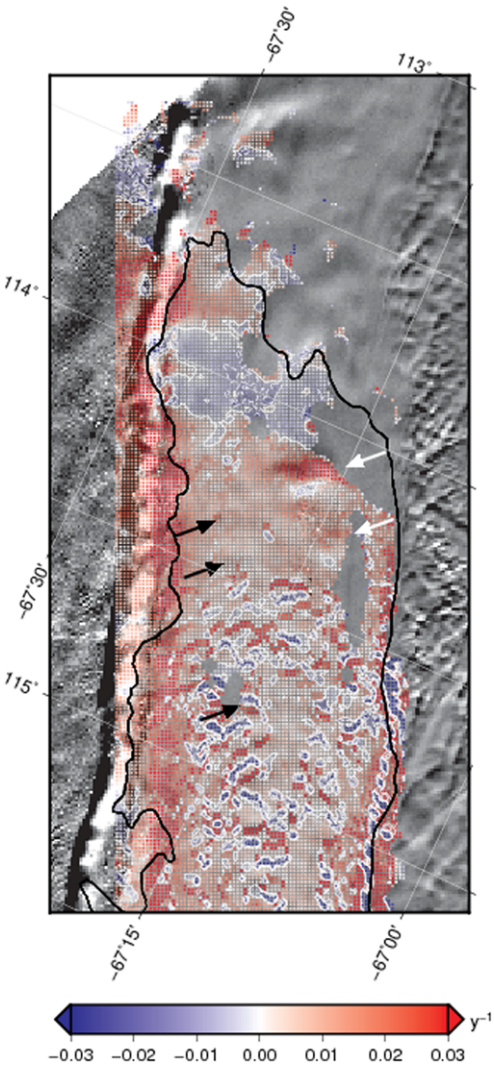

Fig. 4. The TG ice-shelf along-flow strain rate from surface velocity data (Rignot *et al.* 2011); flow compression (negative area, dashed contours around 114°E) upstream of the ice-shelf rumples (white arrows) shows flow retardation associated with basal drag at these rumples. In contrast, the surface undulations (black arrows) are not associated with flow retardation. Also shown is the ASAID grounding line (Bindschadler *et al.* 2011*a*) (thick black).

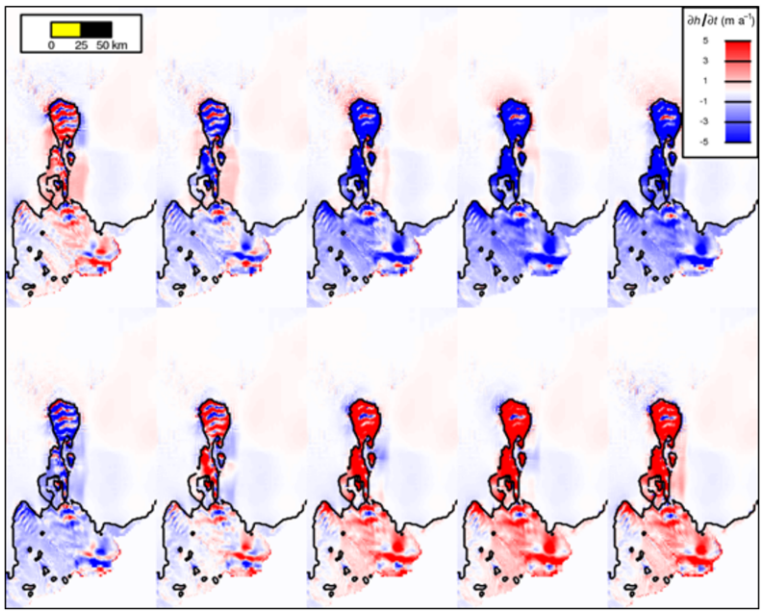

Fig. 5. Series of ice thickness changes for basal melt rate oscillations with an amplitude of 0.5 of the temporal average and a period of 10 years, on the BEDMAP2 grounding line, showing the formation of surface undulations that arise as alternating bands of red and blue.

Discussion

We suggest that the observed velocity and height variations are controlled by ice-shelf back-stress generated around two prominent ice rumples near the southern grounding zone. The reduced back-stress arises from a combination of basal melting around the rumples directly reducing the area of contact, and an indirect, lagged response to thinner ice that is transported over the rumples from increased melting upstream. This back-stress from the rumples has two consequences for the grounded ice stream. First, the drag force of the ice flowing over the rumples provides a back-stress, retarding the flow of the TIS, as indicated by the observed compressive longitudinal strain rate. Secondly, reduction in the back-stress induces dynamic thinning of the ice shelf, with subsequent feedbacks on the grounded flow. Modelling shows the thickness of ice flowing over these rumples is highly sensitive to melt rates. Stronger melting thins the ice and reduces back-stress, leading to an increase in ice velocity (Donnelly 2014) and probable thickness, which is likely to impact the location of the grounding zone. The observed thinning (thickening) appears coincident with faster (slower) velocities, which when considered along with the modelling results suggests a dynamic ice response to the variations in ice-shelf thickness and flow, driven by changes to the retarding (back-stress) forces present in the system due in turn to ocean-driven variability in the basal melt rates.

Coupled ice sheet–shelf modelling (Cornford *et al.* 2015) of the TG system (Donnelly 2014) forced with periodic varying basal melt rates produced associated modulations in ice velocities (differences in the range 90–150 m a^{-1}) controlled by changing back-stress of the ice shelf at rumples (Matsuoka *et al.* 2015), illustrating the connection between basal melt rates, contact topography and flow modulation. The temporal modulation of basal melting also led to train undulations in TIS thickness (Donnelly 2014), analogous to observed TIS surface features in the along-flow direction. The observed spacing suggests variations in melt rates with a period of 6–7 years (Donnelly 2014). Similar undulations have been observed on the Pine Island Glacier ice shelf, where time-varying (in that case, seasonal) basal melt rates have been suggested as the cause (Bindschadler *et al.* 2011*b*).

Interactions between heat exchange across the continental shelf break, atmosphere–ocean processes over the continental shelf and melt-water advection from the Dalton Ice Shelf to TIS combine to produce a range of regimes for the supply of oceanic heat to drive ice-shelf melting (Gwyther *et al.* 2014). For example, a few percent decrease from the average in heat lost to the atmosphere above coastal polynyas can result in TIS melt rates that are double the average. This result is consistent with previous modelling

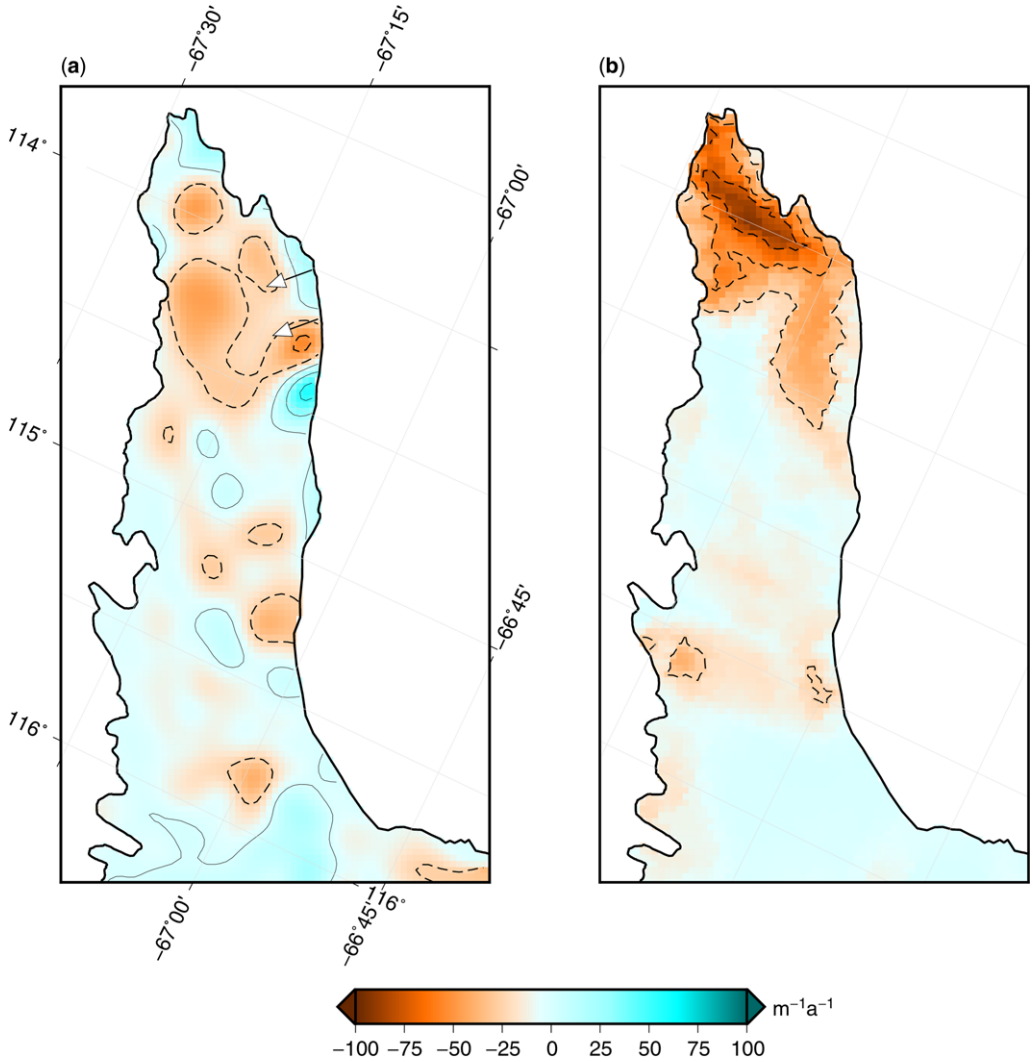

Fig. 6. (**a**) Basal mass flux distribution for the TG ice shelf, calculated from mass flux differences along streamlines based on ice thickness (Roberts *et al.* 2011; Wright *et al.* 2012; Young *et al.* 2011) and surface velocity (Rignot *et al.* 2011) measurements. Results have been plotted with a 5 km Gaussian smoothing kernel. The zero contour is shown (thin black) and 25 m a^{-1} contours (dashed melt, solid refreeze). The locations of ice rumples are indicated (white arrows). Also shown is the ASAID grounding line (Bindschadler *et al.* 2011*a*) (thick black). (**b**) Modelled time-averaged basal melt rates for the 1992–2012 ocean-model simulation.

studies of East Antarctic continental shelf seas, showing the high sensitivity of basal melting to relatively small changes in the amount of oceanic heat that is lost to the atmosphere (Cougnon *et al.* 2013; Khazendar *et al.* 2013). Warm modified Circumpolar Deep Water (MCDW) has been observed on the continental shelf near the TIS (Williams *et al.* 2011), and recent airborne geophysical surveys (including gravity, radar and magnetics) have revealed bathymetric pathways of suitable scale and depth to deliver this water into the ocean-filled cavity beneath the TIS (Greenbaum *et al.* 2015). As a result, modulation of the intrusions of the MCDW to the deepest part of the TIS cavity, near the southern grounding zone, is the most likely scenario driving the strong basal melting and its large variability.

Other plausible mechanisms that could explain the observed variations in velocity include: (1) natural changes in the surface accumulation of ice; or (2) changes in the subglacial hydrology. We doubt either

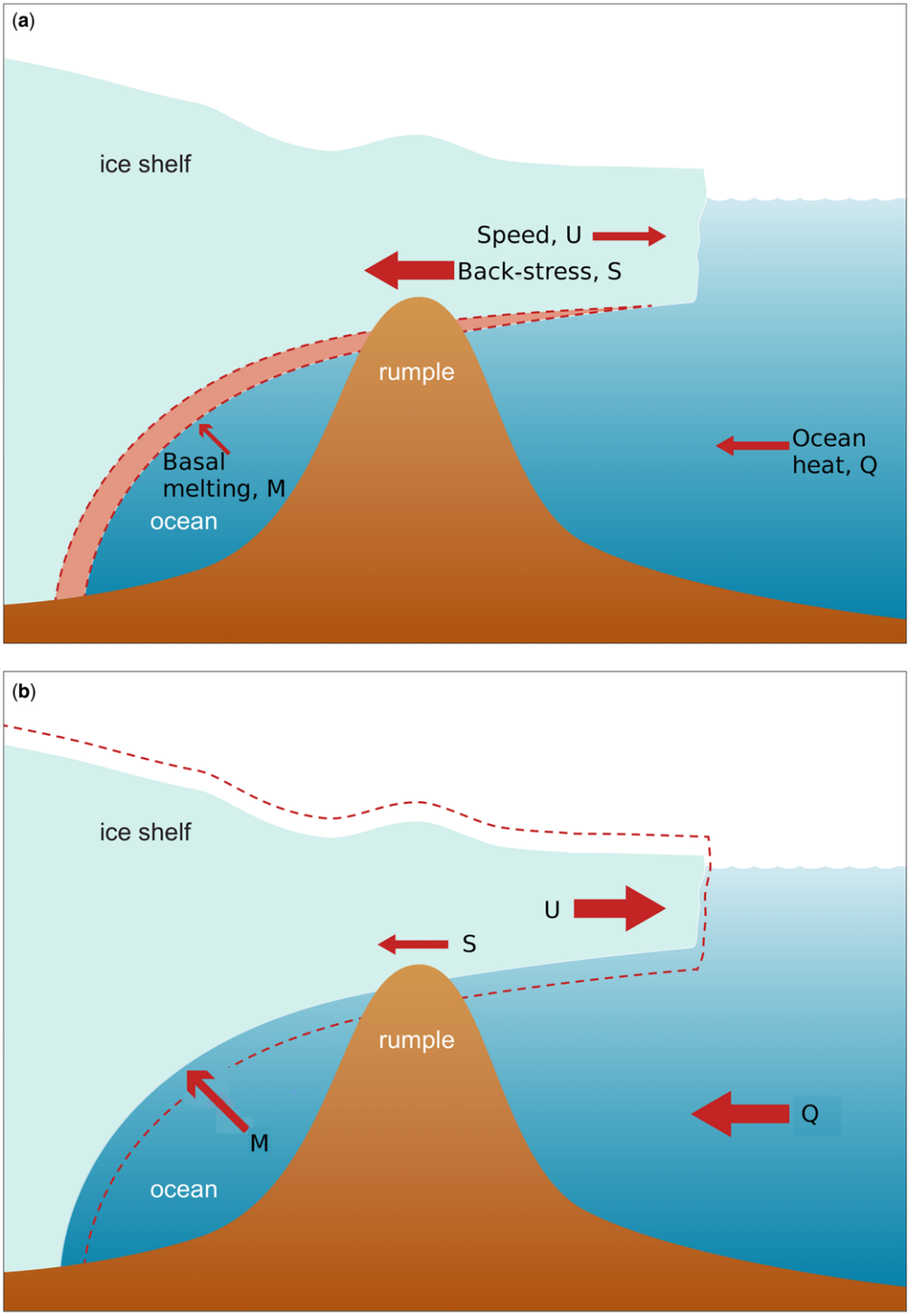

Fig. 7. Schematic of the mechanism whereby the flow of the glacier, *U*, can be (**a**) more, or (**b**) less impeded by the back-stress, *S*, resulting from variable ocean heat flux, *Q*, driving basal melting of the ice shelf, *M*, where the size of the arrows show the relative influence of each component when compared between the two scenarios.

can account for the observations. Increased accumulation could act to make the ice plain more firmly grounded, which could slow both the TG and TIS. However, we expect the adjustment in ice flow in response to accumulation changes to be much slower than observed. Alternatively, there is mounting evidence for an extensive hydrological system in the Aurora Subglacial Basin (Wright *et al.* 2012), including subglacial lake discharge events (Smith *et al.* 2009). Variable basal hydrology is thought to influence glacier dynamics (Stearns *et al.* 2008; Stearns 2011). If the primary mechanism is changing basal hydrology, then this requires relatively less influence of the basal hydrology during the periods 1999–2002 and post-2010. Opportunities for temporary water storage (such as lakes that drain and fill) in the region are limited (Wright *et al.* 2012), suggesting that obvious hydrological-induced ice-flow changes are unlikely to be responsible for the observations reported here (Fig. 7). In addition, no substantial basal water transfer, as has been inferred from satellite altimetry in other regions, has been observed in the TG.

We therefore hypothesis the two main modes of variation of this system are as follows: (A) during periods of cool ocean forcing, basal melt rates are lower and the ice shelf thickens, leading to increasing back-stress at rumples, and the ice flow decreases (Fig. 7a); and (B) during periods of warm ocean forcing, basal melt rates are higher and the ice shelf thins, decreasing the back-stress at rumples, and the ice flow increases (Fig. 7b). Observational evidence does not exist to quantify how promptly the response should be between enhanced melting, which may occur in a region upstream of the rumple, and the advection of ice thickness into the region controlling back-stress that is sufficient to change the ice flow. However, we suggest that a time delay between melting and velocity changes is likely to be small given the proximity of the rumples to the region of deepest ice and highest melting near the grounding line.

Conclusions

From observations and modelling results presented here, we conclude that the variability of the TG over the past two decades is primarily ocean-driven. In particular, the anti-correlation of observed broad-scale elevation changes and modelled melt rates support the timing and overall magnitude of the modelled melt rates, and indicates a high sensitivity of the TIS melt rates to ocean forcing. We argue that the strong variation in melt rate modulates the ice dynamics via the rumples that lie near the grounding line. It is likely that thinning, acceleration and grounding zone retreat of the TG will occur if sub-ice-shelf ocean temperatures, and associated basal melt rates, rise in the future (Sun *et al.* 2016). Our results also demonstrate that the TIS is sensitive to relatively small changes in the supply of oceanic heat into the ice-shelf ocean cavity. In particular, variation in basal melting leads to periodic changes in back-stress at topographical rumples, which act to control ice-shelf velocity. This interplay between ocean forcing, bedrock topography and ice dynamics is analogous to changes observed for the Pine Island region in West Antarctica (Jacobs *et al.* 2011), and if TG responds in the same way, the melting may exceed the ice inflow, leading to sub-ice-shelf cavity enlargement and retreat of the grounding line.

This work was supported by, Australian Antarctic Division projects 3103, 4077, 4287 and 4346, National Computing Infrastructure grant m68, NSF grant ANT-0733025, NASA grant NNX09AR52G (Operation Ice Bridge), NERC grant NE/F016646/1, NERC fellowship NE/G012733/2, the Jackson School of Geoscience, the Jet Propulsion Laboratory and the G. Unger Vetlesen Foundation. This research was also supported by the Australian Government's Cooperative Research Centres Programme through the Antarctic Climate & Ecosystems Cooperative Research Centre. The work is also supported under the Australian Research Council's Special Research Initiative for Antarctic Gateway Partnership SR140300001. Landsat4 and Landsat7 images are courtesy of the United States Geological Survey. This is UTIG contribution No. 2486. Thanks to Benoit Legresy for useful discussions.

References

Aitken, A.R.A., Roberts, J.L. *et al.* 2016. Repeated large-scale retreat and advance of Totten Glacier indicated by inland bed erosion. *Nature*, **533**, 385–389.

Bindschadler, R., Choi, H. *et al.* 2011*a*. Getting around Antarctica: new high-resolution mappings of the grounded and freely-floating boundaries of the Antarctic ice sheet created for the International Polar Year. *The Cryosphere*, **5**, 569–588, https://doi.org/10.5194/tc-5-569-2011

Bindschadler, R., Vaughan, D.G. & Vornberger, P. 2011*b*. Variability of basal melt beneath the Pine Island Glacier ice shelf, West Antarctica. *Journal of Glaciology*, **57**, 581–595, https://doi.org/10.3189/002214311797409802

Brenner, A.C., Bindschadler, R.A., Thomas, R.H. & Zwally, H.J. 1983. Slope-induced errors in radar altimetry over continental ice sheets. *Journal of Geophysical Research*, **88**, 1617–1623.

Chen, J.L., Wilson, C.R., Blankenship, D. & Tapley, B.D. 2009. Accelerated Antarctic ice loss from satellite gravity measurements. *Nature Geoscience*, **2**, 859–862, https://doi.org/10.1038/ngeo694

Cornford, S.L., Martin, D.F. *et al.* 2013. Adaptive mesh, finite volume modeling of marine ice sheets. *Journal of Computational Physics*, **232**, 529–549, https://doi.org/10.1016/j.jcp.2012.08.037

Cornford, S.L., Martin, D.F. *et al.* 2015. Century-scale simulations of the response of the West Antarctic Ice

Sheet to a warming climate. *The Cryosphere*, **9**, 1579–1600, https://doi.org/10.5194/tc-9-1579-2015

Cougnon, E.A., Galton-Fenzi, B.K., Meijers, A.J.S. & Legresy, B. 2013. Modeling interannual dense shelf water export in the region of the Mertz Glacier Tongue (1992–2007). *Journal of Geophysical Research: Oceans*, **118**, 5858–5872, https://doi.org/10.1002/2013JC008790

Davis, C.H. & Ferguson, A.C. 2004. Elevation change of the Antarctic ice sheet, 1995–2000, from ERS-2 satellite radar altimetry. *IEEE Transactions on Geoscience Remote Sensing*, **42**, 2437–2445.

Dee, D.P., Uppala, S.M. *et al.* 2011. The ERA-Interim reanalysis: configuration performance of the data assimilation system. *Quarterly Journal of the Royal Meteorological Society*, **137**, 553–597, https://doi.org/10.1002/qj.828

Donnelly, C. 2014. *Dynamics sensitivity of Totten Glacier, East Antarctica, in Response to Ocean-Driven Change*. School of Geographical Sciences, University of Bristol, Bristol, UK.

Femenias, P. 1996. *ERS QLOPR OPR Range Processing*. ESA/ESRIN Technical Note ER-TN-RS-RA-0022. European Space Agency/European Space Research Institute, Frascati, Italy.

Fretwell, P., Pritchard, H.D. *et al.* 2013. Bedmap2: improved ice bed, surface thickness datasets for Antarctica. *The Cryosphere*, **7**, 375–393, https://doi.org/10.5194/tc-7-375-2013

Galton-Fenzi, B.K., Coleman, R., Hunter, J. & Marsland, S. 2012. Modelling the basal melting marine ice accretion of the amery ice shelf. *Journal of Geophysical Research: Oceans*, **117**, C09031, https://doi.org/10.1029/2012JC008214

Greenbaum, J.S., Blankenship, D.D. *et al.* 2015. Ocean access to a cavity beneath Totten Glacier in East Antarctica. *Nature Geoscience*, **8**, 294–298, https://doi.org/10.1038/NGEO2388

Gwyther, D.E., Galton-Fenzi, B.K., Hunter, J.R. & Roberts, J.L. 2014. Simulated melt rates for the Totten Dalton ice shelves. *Ocean Science*, **10**, 267–279, https://doi.org/10.5194/os-10-267-2014

Jacobs, S.S., Jenkins, A., Giulivi, C.F. & Dutrieux, P. 2011. Stronger ocean circulation increased melting under Pine Island Glacier ice shelf. *Nature Geoscience*, **4**, 519–523, https://doi.org/10.1038/ngeo1188

Khazendar, A., Schodlok, M.P., Fenty, I., Ligtenberg, S. R.M., Rignot, E. & van den Broeke, M.R. 2013. Observed thinning of Totten Glacier is linked to coastal polynya variability. *Nature Communications*, **4**, 2857

Large, W.G. & Yeager, S.G. 2009. The global climatology of an interannually varying air-sea flux data set. *Climate Dynamics*, **33**, 341–364, https://doi.org/10.1007/s00382-008-0441-3

Li, X., Rignot, E., Morlighem, M., Mouginot, J. & Scheuchl, B. 2015. Grounding line retreat of Totten Glacier, East Antarctica, 1996 to 2013. *Geophysical Research Letters*, **42**, 8049–8056, https://doi.org/10.1002/2015GL065701

Li, X., Rignot, E., Mouginot, J. & Scheuchl, B. 2016. Ice flow dynamics and mass loss of Totten Glacier, East Antarctica, from 1989 to 2015. *Geophysical Research Letters*, **43**, 6366–6373, https://doi.org/10.1002/2016GL069173

Matsuoka, K., Hindmarsh, R.C.A. *et al.* 2015. Antarctic ice rises and rumples: their properties and significance for ice-sheet dynamics and evolution. *Earth-Science Reviews*, **150**, 724–745.

Menemenlis, D., Campin, J-M. *et al.* 2008. ECCO2: high resolution global ocean and sea ice data synthesis. *Mercator Ocean Quarterly Newsletter*, **31**, 13–21.

Ólafsdóttir, K.B. & Mudelsee, M. 2014. More accurate, calibrated bootstrap confidence intervals for estimating the correlation between two time series. *Mathematical Geosciences*, **46**, 411–427, https://doi.org/10.1007/s11004-014-9523-4

Paolo, F.S., Fricker, H.A. & Padman, L. 2015. Volume loss from Antarctic ice shelves is accelerating. *Science*, **348**, 327–331, https://doi.org/10.1126/science.aaa0940

Paolo, F.S., Fricker, H.A. & Padman, L. 2016. Constructing improved decadal records of Antarctic ice shelf height change from multiple satellite radar altimeters. *Remote Sensing of Environment*, **177**, 192–205.

Pattyn, F. 2010. Antarctic subglacial conditions inferred from a hybrid ice sheet/ice stream model. *Earth and Planetary Science Letters*, **295**, 451–461, https://doi.org/10.1016/j.epsl.2010.04.025

Pritchard, H.D., Arthern, R.J., Vaughan, D.G. & Edwards, L.A. 2009. Extensive dynamic thinning on the margins of the Greenland Antarctic ice sheets. *Nature*, **461**, 971–975.

Pritchard, H.D., Ligtenberg, S.R.M., Fricker, H.A., Vaughan, D.G., van den Broeke, M.R. & Padman, L. 2012. Antarctic ice-sheet loss driven by basal melting of ice shelves. *Nature*, **484**, 502–505, https://doi.org/10.1038/nature10968

Rignot, E. & Thomas, R.H. 2002. Mass balance of polar ice sheets. *Science*, **297**, 1502–1506, https://doi.org/10.1126/science.1073888

Rignot, E., Bamber, J.L., van den Broeke, M.R., Davis, C., Li, Y., van de Berg, W.J. & van Meijgaard, E. 2008. Recent Antarctic ice mass loss from radar interferometry regional climate modelling. *Nature Geoscience*, **1**, 106–110, https://doi.org/10.1038/ngeo102

Rignot, E., Mouginot, J & Scheuchl, B. 2011. Ice flow of the Antarctic ice sheet. *Science*, **333**, 1427–1430, https://doi.org/10.1126/science.1208336

Rignot, E., Jacobs, S., Mouginot, J. & Scheuchl, B. 2013. Ice-shelf melting around antarctica. *Science*, **341**, 266–270, https://doi.org/10.1126/science.1235798

Roberts, J.L., Warner, R.C. *et al.* 2011. Refined broad-scale sub-glacial morphology of Aurora Subglacial Basin, East Antarctica derived by an ice-dynamics-based interpolation scheme. *The Cryosphere*, **5**, 551–560.

Rousseeuw, P. & Hubert, M. 1997. Recent developments in PROGRESS. *In*: Dodge, Y. (ed.) *L1-Statistical Procedures and Related Topics: Papers from the 3rd International Conference on L1-Norm and Related Methods held in Neuchâtel*, August 11–15, 1997. Institute of Mathematical Statistics Lecture Notes, Monograph Series, **31**, 201–214.

Scambos, T.A., Dutkiewicz, M.J., Wilson, J.C. & Bindschadler, R.A. 1992. Application of image cross-correlation to the measurement of glacier velocity using satellite image data. *Remote Sensing of Environment*, **42**, 177–186.

Scharroo, R. & Visser, P. 1998. Precise orbit determination gravity field improvement for the ERS satellites. *Journal of Geophysical Research: Oceans*, **103**, 8113–8127.

Schoof, C. 2007. Ice sheet grounding line dynamics: steady states, stability, hysteresis. *Journal of Geophysical Research: Earth Surface*, **112**, F03S28, https://doi.org/10.1029/2006JF000664

Shchpetkin, A.F. & McWilliams, J.C. 2005. The regional oceanic modeling system (ROMS): a split-explicit, free-surface, topography-following-coordinate oceanic model. *Ocean Modelling*, **9**, 347–404, https://doi.org/10.1016/j.ocemod.2004.08.002

Shepherd, A. & Wingham, D. 2007. Recent sea-level contributions of the antarctic and greenland ice sheets. *Science*, **315**, 1529–1532.

Smith, B.E., Fricker, H.A., Joughin, I.R. & Tulaczyk, S. 2009. An inventory of active subglacial lakes in Antarctica detected by ICESat (2003–2008). *Journal of Glaciology*, **55**, 573–595, https://doi.org/10.3189/002214309789470879

Stearns, L.A. 2011. Dynamics mass balance of four large East Antarctic outlet glaciers. *Annals of Glaciology*, **52**, 116–126, https://doi.org/10.3189/172756411799096187

Stearns, L.A., Smith, B.E. & Hamilton, G.S. 2008. Increased flow speed on a large East Antarctic outlet glacier caused by subglacial floods. *Nature Geoscience*, **1**, 827–831, https://doi.org/10.1038/ngeo356

Sun, S., Cornford, S.L., Gwyther, D.E., Gladstone, R.M., Galton-Fenzi, B.K., Zhao, L. & Moore, J.C. 2016. Impact of ocean forcing on the Aurora Basin in the 21st–22nd centuries. *Annals of Glaciology*, **57**, 79–86, https://doi.org/10.1017/aog.2016.27

Tamura, T., Ohshima, K.I. & Nihashi, S. 2008. Mapping of sea ice production for Antarctic coastal polynyas. *Geophysical Research Letters*, **35**, L07606, https://doi.org/10.1029/2007GL032903

Timmermann, R., Le Brocq, A. *et al.* 2010. A consistent data set of Antarctic ice sheet topography, cavity geometry, global bathymetry. *Earth System Science Data*, **2**, 261–273, https://doi.org/10.5194/essd-2-261-2010

van Ommen, T.D. & Morgan, V. 2010. Snowfall increase in coastal East Antarctica linked with southwest Western Australian drought. *Nature Geoscience*, **3**, 267–272, https://doi.org/10.1038/ngeo761

Warner, R.C. & Roberts, J.L. 2013. Pine Island Glacier (Antarctica) velocities from Landsat7 images between 2001 and 2011: FFT-based image correlation for images with data gaps. *Journal of Glaciology*, **59**, 571–582, https://doi.org/10.3189/2013JoG12J113

Williams, G.D., Meijers, A.J.S., Poole, A., Mathiot, P., Tamura, T. & Klocker, A. 2011. Late winter oceanography off the Sabrina BANZARE coast (117–128°E), East Antarctica. *Deep-Sea Research Part II: Topical Studies in Oceanography*, **58**, 1194–1210, https://doi.org/10.1016/j.dsr2.2010.10.035

Wingham, D.J., Wallis, D.W. & Shepherd, A. 2009. Spatial temporal evolution of Pine Island Glacier thinning, 1995–2006. *Geophysical Research Letters*, **36**, L17501.

Wright, A.P., Young, D.A. *et al.* 2012. Evidence of a hydrological connection between the ice divide and ice sheet margin in the Aurora Subglacial Basin, East Antarctica. *Journal of Geophysical Research: Earth Surface*, **117**, F01033, https://doi.org/10.1029/2011JF002066

Young, D.A., Wright, A.P. *et al.* 2011. A dynamic early East Antarctic Ice Sheet suggested by ice-covered fjord landscapes. *Nature*, **474**, 72–75.

Zwally, H.J. & Brenner, A.C. 2001. Ice Sheet dynamics mass balance. *In*: Fu, L.L. & Cazenave, A. (eds) *Satellite Altimetry Earth Sciences*. Academic Press, New York, 351–369.

Zwally, H.J., Bindschadler, R.A., Brenner, A.C., Major, J.A. & Marsh, J.G. 1989. Growth of Greenland Ice sheet: measurement. *Science*, **246**, 1587–1589.

Zwally, H.J., Giovinetto, M. *et al.* 2005. Mass changes of the Greenland Antarctic ice sheets shelves contributions to sea-level rise: 1992–2002. *Journal of Glaciology*, **51**, 509–527.